BIOCHEMISTRY
including biophysical chemistry & molecular biology
Article

Biochemistry **2010,** *49,* 8535–8545 8535
DOI: 10.1021/bi1005865

Conformational Changes and Substrate Recognition in *Pseudomonas aeruginosa* D-Arginine Dehydrogenase[†,‡]

Guoxing Fu,[§] Hongling Yuan,[∥] Congran Li,[#] Chung-Dar Lu,[§,⊥] Giovanni Gadda,[∥,§,⊥] and Irene T. Weber*[,§,∥,⊥]

[§]*Departments of Biology,* [∥]*Chemistry, and* [⊥]*The Center for Biotechnology and Drug Design, Georgia State University, Atlanta, Georgia 30303, and* [#]*Laboratory of Pharmacology, Institute of Medicinal Biotechnology, Chinese Academy of Medical Sciences and Peking Union Medical College, Beijing 100050, China*

Received April 16, 2010; Revised Manuscript Received August 19, 2010

ABSTRACT: DADH catalyzes the flavin-dependent oxidative deamination of D-amino acids to the corresponding α-keto acids and ammonia. Here we report the first X-ray crystal structures of DADH at 1.06 Å resolution and its complexes with iminoarginine ($DADH_{red}$/iminoarginine) and iminohistidine ($DADH_{red}$/iminohistidine) at 1.30 Å resolution. The DADH crystal structure comprises an unliganded conformation and a product-bound conformation, which is almost identical to the $DADH_{red}$/iminoarginine crystal structure. The active site of DADH was partially occupied with iminoarginine product (30% occupancy) that interacts with Tyr53 in the minor conformation of a surface loop. This flexible loop forms an "active site lid", similar to those seen in other enzymes, and may play an essential role in substrate recognition. The guanidinium side chain of iminoarginine forms a hydrogen bond interaction with the hydroxyl of Thr50 and an ionic interaction with Glu87. In the structure of DADH in complex with iminohistidine, two alternate conformations were observed for iminohistidine where the imidazole groups formed hydrogen bond interactions with the side chains of His48 and Thr50 and either Glu87 or Gln336. The different interactions and very distinct binding modes observed for iminoarginine and iminohistidine are consistent with the 1000-fold difference in k_{cat}/K_m values for D-arginine and D-histidine. Comparison of the kinetic data for the activity of DADH on different D-amino acids and the crystal structures in complex with iminoarginine and iminohistidine establishes that this enzyme is characterized by relatively broad substrate specificity, being able to oxidize positively charged and large hydrophobic D-amino acids bound within a flask-like cavity.

All the standard amino acids except glycine can exist as either L- or D-optical isomers. L-Amino acids are predominant in proteins synthesized by all living organisms. D-Amino acids are important for bacteria as fundamental elements of the bacterial cell wall peptidoglycan layer (*1*). Several D-amino acids, D-leucine, D-methionine, D-tyrosine, and D-tryptophan, were recently reported to regulate disassembly of bacterial biofilms (*2*). Also, specific D-amino acids have been discovered in many physiological processes in vertebrates, including humans (*3*). Dunlop et al. identified D-aspartate in the brain and other tissues of mammals and suggested it may play a role in regulating the development of these organs (*4*). D-Serine was identified at significant levels in rat brain, at about a third of the level of L-serine (*5*). Moreover, D-serine in the rat brain is distributed in close association with *N*-methyl-D-aspartate (NMDA), and it may act as an endogenous agonist of the NMDA receptor in mammalian brains (*5*).

Conversion of L- and D-amino acids in living organisms is commonly catalyzed by racemases. Various amino acid racemases have been identified in bacteria, archaea, and eucaryotes including mammals. These racemases are classified into two groups: pyridoxal 5′-phosphate- (PLP-) dependent and independent enzymes (*3*). In mammals, D-serine racemases and D-aspartate racemases are the most intensively studied enzymes due to their involvement in cell aging and neural signaling (*6*, *7*). In bacteria, D-amino acids are deaminated by flavin-dependent dehydrogenases (*8*), allowing the bacteria to grow using D-amino acids as the sole carbon, nitrogen, and energy source, in a concentration-sensitive manner, since some D-amino acid analogues have toxic effects on bacterial growth (*9*, *10*).

Pseudomonas aeruginosa, an opportunistic human pathogen, can grow with D-arginine as the sole source of carbon and nitrogen (*11*). D- to L-arginine racemization by two coupled dehydrogenases serves as prerequisite of D-arginine utilization through L-arginine catabolic pathways (*12*, *13*). One enzyme is an FAD-dependent catabolic DADH,[1] and the other is an NAD(P)H-dependent anabolic LADH. DADH catalyzes the conversion of D-arginine into 2-ketoarginine and ammonia, and LADH converts 2-ketoarginine to L-arginine. In order to understand the reaction mechanism and substrate specificity of DADH, the crystal structure of DADH was determined at the atomic resolution of 1.06 Å, while the structures of DADH crystallized in the presence of D-arginine and D-histidine were both determined at 1.30 Å resolution. Well-defined electron density for the noncovalently bound FAD and imino intermediate of the reaction allowed

[†]This work was supported in part by NSF-CAREER Award MCB-0545712 (G.G.), NSF Grant 0950217 (C.L.), and the Georgia State University Molecular Basis of Disease Fellowship (G.F.).

[‡]The atomic coordinates and structure factors have been deposited in the Protein Data Bank with accession codes 3NYC for DADH, 3NYE for $DADH_{red}$/iminoarginine, and 3NYF for $DADH_{red}$/iminohistidine.

*Address correspondence to this author. Phone: (404) 413-5411. Fax: (404) 413-5301. E-mail: iweber@gsu.edu.

[1]Abbreviations: DADH, D-arginine dehydrogenase; LADH, L-arginine dehydrogenase; DAAD, D-amino acid dehydrogenase; pDAAO, porcine D-amino acid oxidase; hDAAO, human D-amino acid oxidase; LAAO, L-amino acid oxidase; PMS, phenazine methosulfate; rmsd, root-mean-square deviation.

© 2010 American Chemical Society
Published on Web 09/01/2010

detailed analysis of the enzyme active site. A loop region with alternative conformations was identified in the DADH structure and is involved in substrate binding. Very distinct binding modes were observed for iminoarginine and iminohistidine, in agreement with detailed kinetic analysis on substrate specificity reported previously (*14*) and in this paper. The structural characteristics described here provide insights into substrate recognition and the catalytic reaction mechanism of DADH.

EXPERIMENTAL PROCEDURES

Materials. D-Amino acids and L-amino acids were from Alfa Aesar and Sigma-Aldrich (St. Louis, MO). Phenazine methosulfate (PMS) and phenylmethanesulfonyl fluoride (PMSF) were obtained from Sigma-Aldrich (St. Louis, MO). All of the other reagents were of the highest purity commercially available.

Expression and Purification of DADH and SeMet-DADH. Hexahistidine-tagged DADH was expressed in *Escherichia coli* TOP10 and purified as described previously (*13*). No FAD was added during expression and purification. The selenomethionine (SeMet) DADH protein was prepared following a protocol with slight modifications as described in a previous study (*15*). DTT (10−20 mM) was incorporated in the buffer throughout the purification steps in order to avoid oxidation of selenium. Mass spectrometry confirmed that about 88% of the eight methionines were replaced by Se-Met.

Crystallization and X-ray Data Collection. Purified DADH and SeMet-DADH were concentrated to 6 and 3 mg/mL, respectively, in 50 mM Tris at pH 7.5. Crystals were grown by the hanging drop vapor diffusion method using a well solution of 0.1 M 2-(*N*-morpholino)ethanesulfonic acid (MES) pH 6.5−7.0, 5% glycerol, and 6−10% (w/v) PEG6000. Crystals can grow to a size of 0.1−0.2 mm^3 within 2 weeks. DADH was cocrystallized with D-arginine or D-histidine under similar conditions using a 1:10 molar ratio of the enzyme (~0.15 mM) to substrate. The crystals were soaked in the reservoir solution with 20% glycerol as cryoprotectant for ~1 min and frozen immediately in liquid nitrogen. X-ray data were collected at 100 K on beamline 22-ID of the Southeast Regional Collaborative Access Team (SER-CAT) at the Advanced Photon Source, Argonne National Laboratory. Single-wavelength anomalous diffraction (SAD) data for SeMet-DADH were collected at the wavelength of 0.97182 Å (high energy remote) on beamline 22-BM of SER-CAT at Argonne National Laboratory.

Structure Determination and Model Refinement. The X-ray data were integrated and scaled using HKL2000 (*16*). Program SGXPRO was used to perform phasing and automatic tracing with scaled but unmerged SeMet-DADH data (*17*). With this approach, 331 of the 381 residues (375 amino acids residues of the enzyme and the N-terminal hexahistidine tag) (~87%) were successfully built. This model was then used for automated model building by ARP/WARP (*18*), in which 96% of the structure was fit. The structure of SeMet-DADH was then employed to solve the native DADH data set (1.06 Å) by molecular replacement using PHASER (*19*) in the CCP4i suite of programs (*20*). Notably, all of the FAD atoms were distinctly visible in the electron density maps. FAD was refined with 100% occupancy. The structure of DADH was used to solve the structures of DADH cocrystallized with D-arginine or D-histidine by molecular replacement. Crystal structures were refined with SHELX97 (*21*). Manual adjustments and rebuilding were performed using the molecular graphics program COOT (*22*). The structures of DADH cocrystallized with D-arginine and D-histidine showed difference density for iminoarginine and iminohistidine, respectively, bound at the enzyme active site, as observed for D-amino acid oxidase crystallized in the presence of D-tryptophan (*23*). The D-amino acids are converted enzymatically to imino acids (R−C=NH), which then dissociate from the enzyme and are hydrolyzed to the final keto acids (R−C=O) in a nonenzymatic reaction. The iminoarginine was refined with 100% occupancy, while two alternate conformations were visible for the iminohistidine that refined to relative occupancies of 60% and 40%. Further analysis showed that the structure of DADH, which was crystallized without added D-amino acids, contained extra density for a low occupancy iminoarginine adjacent to a disordered loop showing two alternate conformations. This structure was refined with two conformers corresponding to 70% occupancy of a ligand-free, open conformation DADH and 30% occupancy of iminoarginine bound to a closed conformation of DADH. Higher peaks in the $2F_o - F_c$ electron density ($> 5\sigma$) were observed for the two main-chain oxygen atoms of iminoarginine, while smaller density peaks ($\sim 1.3\sigma$) were visible for other atoms. Therefore, in the ligand-free conformation, two water molecules were refined near the carboxylate oxygen atoms of iminoarginine. Solvent molecules were inserted at stereochemically reasonable positions based on the peak height of the $2F_o - F_c$ and $F_o - F_c$ electron density maps, hydrogen bond interactions, and interatomic distances. Anisotropic *B*-factors were refined for all of the structures. Hydrogen atom positions were included in the last stage of refinement using all data.

Sequence similarity searches were performed using BLAST (*24*). Protein structures were superimposed on Cα atoms by using the secondary structure matching (SSM) module in COOT (*25*). Figures of the structures were generated with PYMOL (http://www.pymol.org).

Enzyme Assay. The determination of the apparent steady-state kinetic parameters was carried out by measuring initial rates of reaction with an oxygen electrode at varying concentrations of the D-amino acid substrate and a fixed concentration of 1 mM for PMS as electron acceptor. The reaction mixture (1 mL) was first equilibrated with organic substrate and PMS at the desired concentrations before the reaction was started by the addition of DADH. Enzyme assays were conducted in 20 mM Tris-HCl, pH 8.7, 25 °C. All reaction rates are expressed per molar concentration of enzyme-bound flavin.

RESULTS

Overall Structure of DADH. The DADH was crystallized without the addition of FAD or D-amino acid, and the structure was solved in the orthorhombic space group $P2_12_12_1$ with one molecule per asymmetric unit using single anomalous dispersion (SAD) phasing and automated tracing. The structure was refined to an *R*-factor of 13.2% at 1.06 Å resolution. Structures were obtained also for DADH crystallized with substrates D-arginine or D-histidine under similar conditions. The structures were solved in the same space group $P2_12_12_1$ by using molecular replacement with the DADH structure as a template and were both determined at the resolution of 1.30 Å and refined to *R*-factors of 13.4% and 12.8%, respectively. The crystallographic data and refinement statistics are summarized in Table 1. In the three structures, all 375 DADH residues and N-terminal hexahistidine tag were defined clearly in the electron density map. Further analysis of the N-terminus of the structure revealed that

Table 1: Crystallographic Data Collection and Refinement Statistics

	SeMet-DADH	DADH	DADH/D-Arg	DADH/D-His
data collection statistics				
redox state of flavin		mixed[a]	reduced	reduced
wavelength (Å)	0.97182[b]	0.99999	1.00000	1.00000
space group	$P2_12_12_1$	$P2_12_12_1$	$P2_12_12_1$	$P2_12_12_1$
a (Å)	62.65	62.18	62.17	62.10
b (Å)	78.21	78.08	78.43	78.15
c (Å)	89.47	89.72	89.95	89.59
resolution range (Å)	50−1.50	50−1.06	50−1.30	50−1.30
total observations	1016247	1258212	600949	627618
unique reflections	70270	190545	98021	97110
completeness	99.7 (98.0)[c]	96.2 (69.1)	90.6 (53.9)	90.4 (54.7)
$\langle I/\sigma(I)\rangle$	27.6 (16.6)	26.5 (2.3)	18.5 (2.7)	31.8 (3.2)
R_{sym} (%)	7.6 (18.1)	6.2 (41.4)	8.2 (37.3)	4.9 (30.6)
figure of merit	0.72			
f'	−4.2234			
f''	3.7853			
refinement statistics				
resolution range (Å)		10−1.06	10−1.30	10−1.30
R_{work} (%)		13.2	13.4	12.8
R_{free} (%)		15.9	16.6	16.3
mean B-factor (Å^2)		16.0	15.9	17.5
protein		14.4	14.6	16.1
FAD		7.3	6.5	8.3
ligand		29.5	37.0	16.3
water		27.9	29.7	31.8
no. of atoms				
protein		3102	2961	2971
FAD		53	53	53
ligand		12	12	22
water		467	358	367
rms deviations				
bond length (Å)		0.017	0.013	0.012
angle[d]		0.035	0.031	0.030

[a]The DADH structure contains both ligand-free and product-bound conformations. [b]The SeMet-DADH data were collected at the wavelength of high energy remote. [c]Values in parentheses are given for the highest resolution shell. [d]The angle rmsd in SHELX97 is indicated by distance in Å.

the His-tag residues form several direct or water-mediated polar interactions with residues from symmetry-related molecules, which stabilize the flexible terminus. Overall, the three structures are almost identical with pairwise rmsd values of 0.10−0.11 Å for 381 Cα atoms. The protein folds into two domains: an FAD-binding domain and a substrate-binding domain (Figure 1). The FAD-binding domain includes residues 1−82, 147−217, and 309−375. It consists of a central six-stranded β-sheet surrounded by five α-helices on one side and a three-stranded antiparallel β-sheet with two α-helices on the other side. The substrate-binding domain is formed by residues 83−142 and 218−297 and consists of an eight-stranded β-sheet and two short antiparallel β-strands forming a sandwich surrounded by four α-helices. The substrate-binding site was identified near the *re* face of the FAD 7,8-dimethylisoalloxazine ring at the interface of the two domains.

FAD-Binding Site. DADH contains a noncovalently bound FAD cofactor as identified in the X-ray crystal structures. All non-hydrogen atoms of the FAD were clearly visible in the electron density map (Figure 2A). The flavin adopts an elongated conformation with the adenine ring buried inside the FAD-binding domain and the isoalloxazine ring located at the interface of the two domains. The adenine portion of the cofactor points toward the flavin binding domain and the 7,8-dimethylisoalloxazine ring is directed toward the interface of the two domains, similar to the FADs observed in other flavin-dependent enzymes, such as L-proline dehydrogenase (*26*), D-amino acid oxidase (*27*),

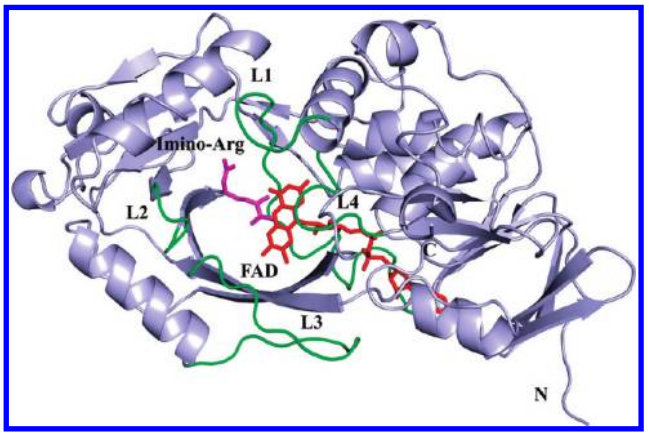

FIGURE 1: Overall structure of DADH with iminoarginine. The DADH structure is shown in cartoon representation. Iminoarginine and cofactor FAD are shown as sticks and colored magenta and red, respectively. Loops that contribute to the active site are colored green.

and L-amino acid oxidase (*28*, *29*). As illustrated in Figure 2B, the ribose ring moiety has hydrogen bond interactions with the side chain of Glu32, two water molecules, and the main-chain atoms of Arg33 and Ala171. Numerous hydrogen bonds are present between the phosphate groups and the peptidyl atoms of Ala14, Thr42, Gly331, and four water molecules. The central part of the

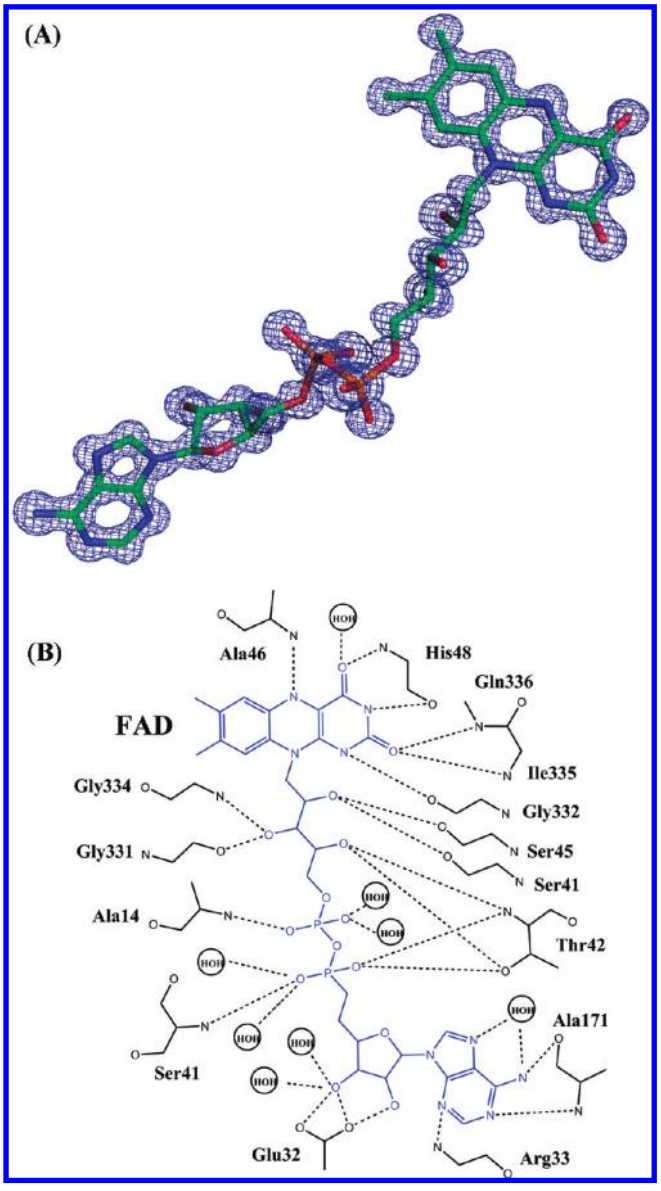

FIGURE 2: (A) The $2F_o - F_c$ electron density map of FAD contoured at 2σ illustrates the high quality of the 1.06 Å resolution structure. FAD (colored by element type) adopts an elongated conformation. (B) Schematic diagram of the flavin−apoprotein interactions in the product-bound DADH conformation. Hydrogen bonds are indicated by dashed lines. The flavin cofactor is colored blue. For clarity, H atoms are not shown.

conserved glycine-rich sequence GXGXXG in the N-terminal region of the polypeptide is part of an α-helix (residues 13−25) that points toward the phosphate group and is assumed to contribute to the stabilization of the two negative charges of the diphosphate (*30*). The 2′-OH and 4′-OH of the ribityl moiety of the cofactor establish hydrogen bond interactions with Ser41, Thr42, and Ser45. The 3′-OH group interacts with peptidyl atoms of Gly331 and Gly334.

The 7,8-dimethylisoalloxazine is sharply bent between the two planes containing the benzene and pyrimidine moieties, defining a 15° angle along the N5−N10 axis. This conformation is in agreement with several other crystallographic structures of flavin-dependent enzymes in which the flavin is in the reduced state (*31*). The pyrimidine portion of the 7,8-dimethylisoalloxazine ring interacts through several hydrogen bonds with backbone atoms of the protein (i.e., C2=O atom with N atom of Ile335, Gln336, N3−H atom with the O atom of His48 and a water molecule, and C4=O atom with the N atom of His48). The benzene portion of the 7,8-dimethylisoalloxazine ring is excluded from solvent and forms van der Waals contacts with Arg44, Arg222, Trp301, Gly303, and Arg305.

Interactions of DADH with Iminoarginine. In order to investigate the structural basis for the substrate recognition of DADH, the enzyme was crystallized with D-arginine that was converted to iminoarginine. Iminoarginine binds with the plane formed by its Cα atom, carboxylate group, and imino group approximately parallel to the *re* face of the flavin, while the side chain points away from the FAD (Figure 3A). The α-carbon of the iminoarginine is 3.3 Å away from the FAD N5 atom, which is compatible with direct involvement of these atoms in the arginine oxidation catalyzed by DADH. The iminoarginine imino group is pointed out of the plane of the carboxylate atoms and can form a 2.9 Å long hydrogen bond interaction with the FAD O4 atom (Figure 3B). Several DADH residues form extensive polar interactions with the two main-chain carboxyl oxygen atoms of iminoarginine that anchor the ligand in the active site. One of the iminoarginine carboxyl oxygen atoms forms hydrogen bonds with the side-chain hydroxyl of Tyr53, the guanidinium side chain of Arg305, and the carbonyl oxygen of Gly332. The other ligand carboxyl oxygen forms hydrogen bonds with the side-chain nitrogen of Arg222 and side-chain hydroxyl of Tyr249. Two water molecules are located near the ligand imino group and form a hydrogen bond network extending to the imidazole side chain of His48. The side chain of iminoarginine forms hydrophobic interactions with the Val242 side chain and a hydrogen bond interaction with the hydroxyl of Thr50. A strong ionic interaction (2.5 Å distance between pairs of O and N atoms) was observed between the guanidinium group of iminoarginine and the carboxylate group of Glu87. Hence, Glu87 may play an important role in the high specificity of DADH for D-arginine, in agreement with the kinetic analysis on substrate specificity of DADH reported previously (*14*) and performed in this study (*vide infra*).

Interactions of DADH with Iminohistidine. The structure of DADH was also determined for crystals grown in the presence of D-histidine, thereby yielding a $DADH_{red}$/iminohistidine complex. The iminohistidine binds to the DADH active site in two discrete conformations with clear density for the overlapping Cα atoms and carboxylate groups and weaker density for the alternate positions of the side chains (Figure 3C). The two iminohistidine conformations are related by a rotation of approximately 180°. In fact, there might be two additional conformations that are indistinguishable in this structure due to the potential 180° rotation of the imidazole ring. The imidazole orientation showing more hydrogen bond interactions with DADH is illustrated in Figure 3D. The main-chain atoms of conformation A (60% occupancy) lie nearly parallel to the isoalloxazine ring of FAD, whereas its imidazole side chain is rotated by about 30°. The iminohistidine atoms of conformation B (40% occupancy) all lie on the same plane. DADH residues Tyr53, Arg222, Tyr249, Arg305, and Gly332 form conserved polar interactions with the ligand main-chain oxygen atoms in both conformations (Figure 3D). The imino group of the ligand forms a polar interaction with Gly332 in conformation A and with the hydroxyl of Tyr249 in conformation B. In both conformations the side chain of iminohistidine forms hydrogen bonds with the side chain of His48 and the hydroxyl of Thr50. The imidazole group also interacts with the side chain of Glu87

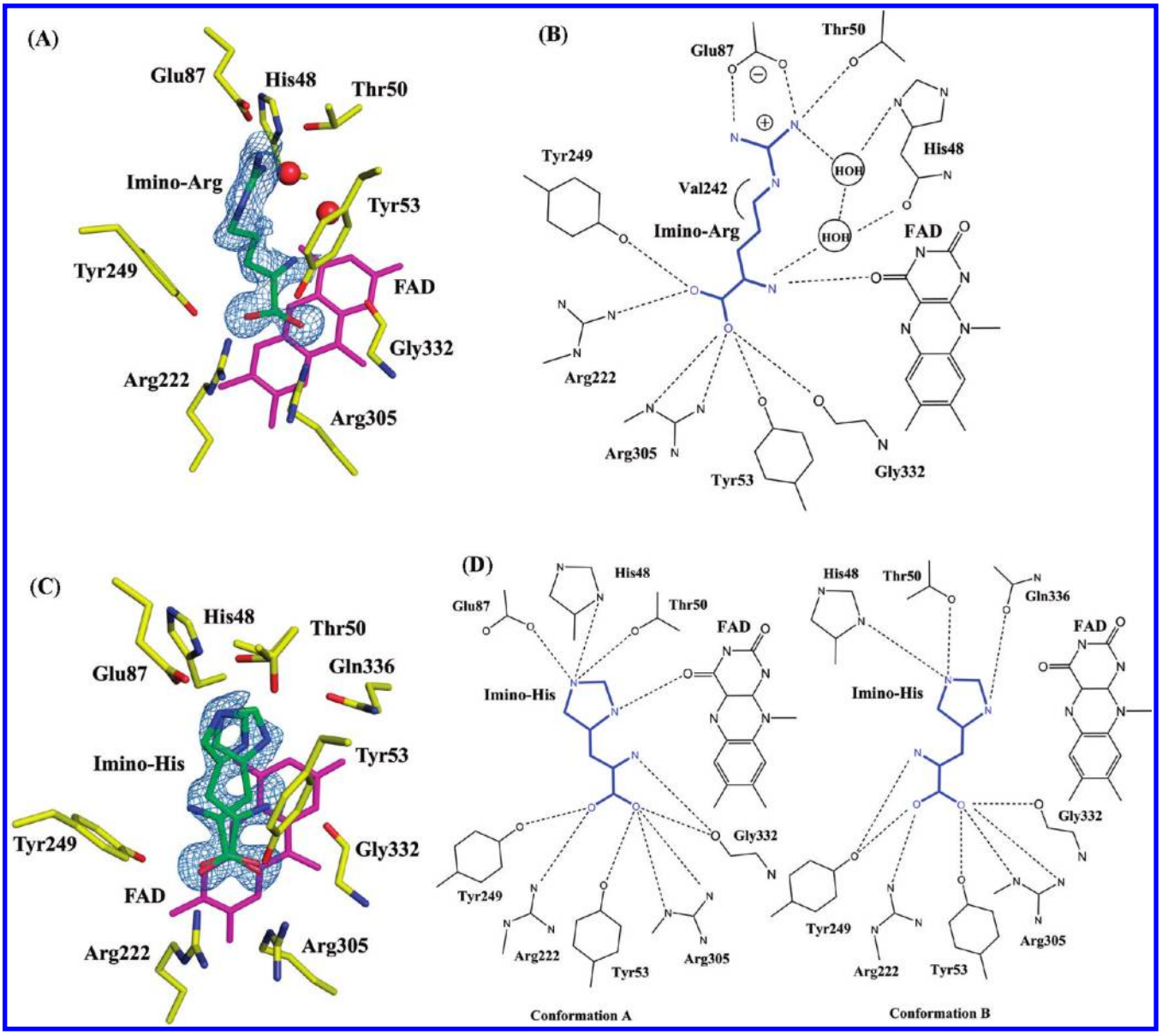

FIGURE 3: DADH interactions with iminoarginine (A, B) and iminohistidine (C, D). Carbons are colored yellow for DADH active site residues and green for the imino acids. FAD is represented by its isoalloxazine ring in magenta. The $F_o - F_c$ omit map of the ligand is indicated as blue mesh and contoured at 3σ. Dashed lines represent hydrogen bonds and ionic interactions.

and the O4 of FAD in conformation A and the side chain of Gln336 in conformation B. When the imidazole is rotated by 180° the interactions with His48, Thr50, and Gln336 are retained for conformation B. The interactions of conformation A with Glu87 and FAD are lost, however, suggesting they are not critical since they appear in only one of four possible conformations of iminohistidine.

Conformational Flexibility of the Active Site. No substrate or other ligand was added to the protein solution during crystallization of the DADH. However, the solved ligand-free structure contained weaker density at the substrate-binding site that was fit by 30% occupancy of the iminoarginine reaction product. It is possible that the ligand was trapped during the bacterial expression of the protein, as observed for other enzymes; for example, a tetrahedral reaction intermediate was discovered in the crystal structure of bacterial Est30 (*15*). The iminoarginine lies adjacent to residues 50−56 of loop L1 with two alternate conformations that were refined with 0.7/0.3 relative occupancy (Figure 4A). This loop had a single well-defined conformation in the electron density for structures of DADH with iminoarginine and iminohistidine that corresponds to the lower occupancy conformation in the ligand-free structure. Therefore, the crystal structure of DADH contains both ligand-free and product-bound conformations, which suggests that a conformational change occurs in the adjacent loop regions upon binding of the substrate. Comparison of the two conformations of DADH revealed distinct changes in two regions of loop L1: residues 50−56 adjacent to the imino product and residues 45−47 near the flavin ring of FAD.

One of the major conformational changes between the ligand-free and the product-bound conformations in the DADH structure was observed at the substrate-binding site for residues 50−56 of loop L1 region (Figure4B). Four loops (L1, residues 33−56; L2, 244−248; L3, 261−276; L4, 329−336) form a flask-like substrate-binding pocket. The binding pocket has a small entrance but expands at the bottom near FAD. The iminoarginine product binds to DADH in a similar manner as observed in the structures of pDAAO/iminotryptophan (*23*) and hDAAO/iminoserine (*32*). In the ligand-free conformation, the side chain

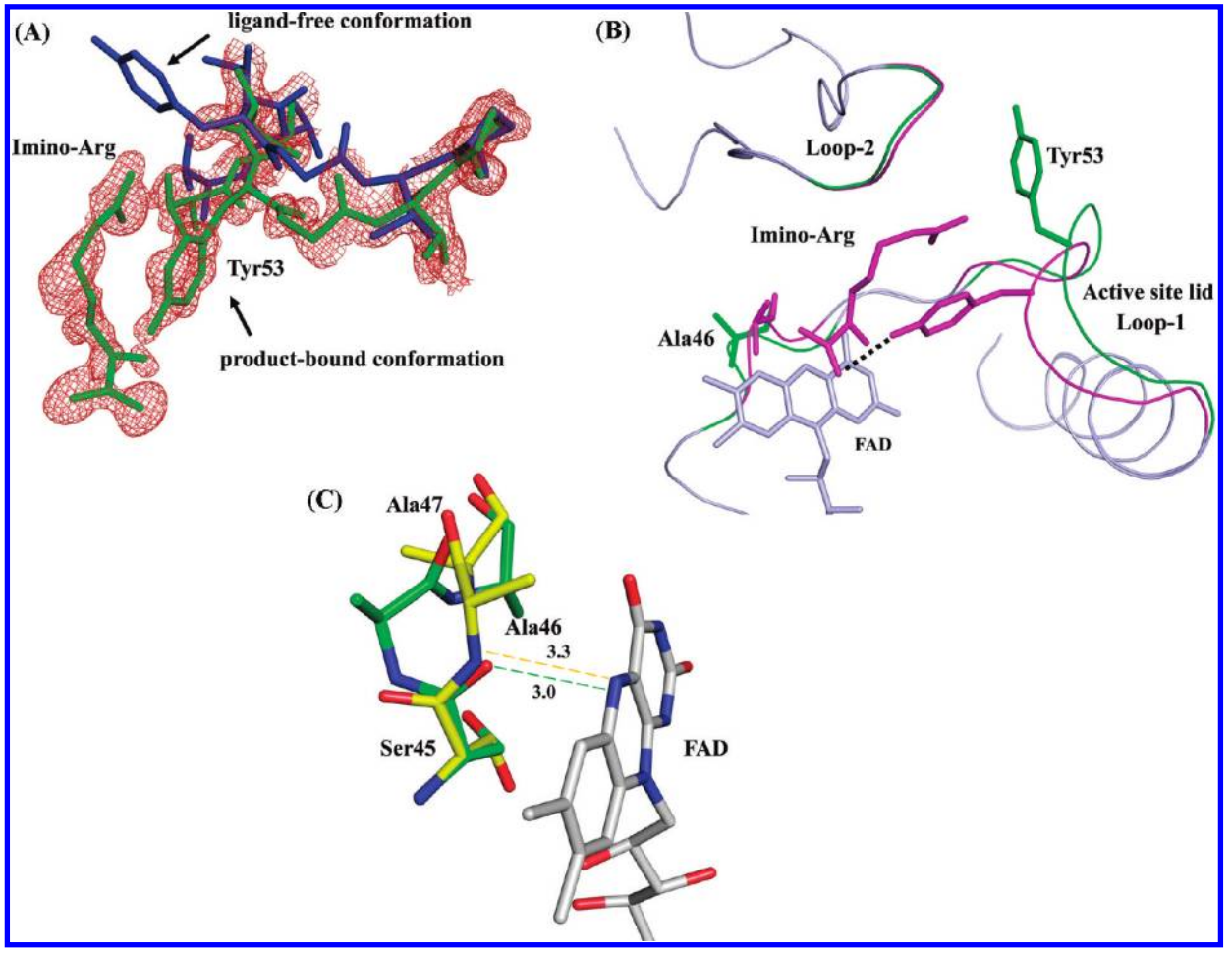

FIGURE 4: Conformational flexibility of DADH structure. (A) The DADH structure comprises two conformers: a 30% occupied population with iminoarginine product and a 70% one without ligand. The iminoarginine and its adjacent loop region with low occupancy (product-bound conformation) are shown as green sticks. The $F_o - F_c$ omit map of this region (red mesh) is contoured at 2.5σ. The corresponding loop region with high occupancy (ligand-free conformation) is shown as blue sticks. (B) Comparison of ligand-free conformation (green) and product-bound conformation (magenta) at loop L1 (residues 33−56) and L2 (residues 244−248) regions in DADH structure. Ala46, Tyr53, and iminoarginine are represented as sticks. A hydrogen bond (black dotted line) is formed between Tyr53 and iminoarginine in the product-bound conformation. (C) Conformational change of residues Ser45-Ala46-Ala47 at the *si* face of flavin ring. Ser45 in the ligand-free conformation (green carbon atoms) forms a 3.0 Å hydrogen bond with the FAD N5 atom (gray carbon atoms). Ala46 forms a 3.3 Å long hydrogen bond with the N5 atom of FAD in the product-bound conformation (yellow carbon atoms).

of Tyr53 points away from the active site and forms a hydrogen bond with Thr137, whereas in the structure of the product-bound enzyme, the aromatic ring of Tyr53 moves into the active site and forms hydrogen bonds with the carboxyl oxygen of the imino acid and also the side chains of Glu246 and Arg305. Other residues also form different interactions in the two conformations of this loop. In the ligand-free conformation, the side chain of Thr50 forms hydrogen bonds with Asp39 and Ala52, while Gly54 and Thr55 both form polar interactions with Arg59. In the product-bound conformation, Thr50 interacts with Glu87 and Gln336, and its main-chain peptidyl oxygen forms a hydrogen bond with the main-chain amide of Tyr53. The hydroxyl side chain of Thr55 forms a hydrogen bond with Asp312. The interactions of Tyr53 and Thr50, in particular, stabilize the ligand bound in the active site, suggesting that this flexible loop L1 region may act as a lid controlling substrate accessibility to the active site. The shape and flexibility of the active site enable DADH to control the entrance of substrates and accommodate a variety of substrates.

The second region showing significant differences in the ligand-free and product-bound conformations comprised residues 45−47 at the N-terminal end of loop L1, which is located at the *si* face of the flavin ring (Figure 4C). This region possesses two conformations in the DADH structure and shows a single well-defined conformation in the structures of DADH with high occupancy products. In the ligand-free conformation, the Ser45 hydroxyl group forms a hydrogen bond with the flavin N5 atom, and the side chain of Ala46 is pointed away from FAD. In the product-bound conformation, this region is flipped about 90° with the side chain of Ser45 pointed away from FAD and the Ala46 side chain approaching closer to the FAD. This structural change causes the loss of the hydrogen bond interaction between Ser45 and FAD, and instead, a new hydrogen bond is formed between the main-chain amide of Ala46 and the N5 of FAD. A similar interaction was reported between the Ala49 of pDAAO and its FAD N5 atom (*23*, *27*). Due to the conformational changes of residues 50−56 and 45−47 in the loop L1 region, the active site of DADH shrinks by about 3.8 Å when the product is bound. The distances between the Cα atoms of Ala46 and Tyr53 are 17.5 and 13.7 Å in the ligand-free conformation and product-bound conformation, respectively (Figure 4B). Loop L2 also has a slight conformational change and moves about 0.7 Å closer to loop L1 based on the distances between the Cα atoms of loop L1 Tyr53 and loop L2 Asp245.

Table 2: Steady-State Kinetics of DADH[a]

substrates	k_{cat}/K_m, M^{-1} s^{-1}	k_{cat}, s^{-1}	K_m, mM
D-arginine	$(3.4 \pm 0.3) \times 10^6$	204 ± 3	0.06 ± 0.01
D-lysine	$(5.3 \pm 0.2) \times 10^5$	141 ± 3	0.26 ± 0.01
D-tyrosine	27600 ± 3800	23 ± 1	0.8 ± 0.1
D-methionine	14800 ± 600	154 ± 3	10 ± 1
D-phenylalanine	6900 ± 300	75 ± 3	11 ± 1
D-histidine	3140 ± 30	35 ± 1	11 ± 1
D-leucine	515 ± 60	6.4 ± 0.3	12 ± 1
D-proline	420 ± 10	–[b]	–
D-tryptophan	245 ± 3	–	–
D-isoleucine	195 ± 3	–	–
D-valine	47 ± 1	–	–
D-alanine	41 ± 1	–	–
D-glutamine	186 ± 3	–	–
D-asparagine	16 ± 1	–	–
D-serine	3.8 ± 0.1	–	–
D-threonine	0.75 ± 0.01	–	–
D-glutamate	–	–	–
D-asparate	–	–	–
L-arginine	–	–	–
glycine	–	–	–
D-cysteine	nd[c]	nd	nd

[a]Enzyme activity was measured at varying concentrations of substrate and 1 mM PMS in 20 mM Tris-HCl, pH 8.7, at 25 °C. [b]Cannot be saturated with the substrate; thereby k_{cat} and K_m values are not reported. [c]Not determined. PMS was reduced by cysteine.

Substrate Specificity. The steady-state kinetic parameters were determined by measuring initial rates of reaction with various D-amino acids in 20 mM Tris-HCl, pH 8.7 at 25 °C. With both D-arginine and D-histidine as substrates for DADH, the K_m value for PMS is ~10 μM at pH 8.7; moreover, with both substrates the enzyme displays a ping-pong bi-bi steady-state kinetic mechanism (H. Yuan and G. Gadda, unpublished results). The concentration of the electron acceptor PMS was kept fixed at 1 mM PMS, ensuring saturation of the enzyme during steady-state turnover. The k_{cat} values determined in this study were larger than those previously reported (*14*), which were expressed per molar concentration of protein rather than enzyme-bound flavin. As illustrated in Table 2 the enzyme showed substrate preferences for amino acids with positively charged side chains, of which D-arginine appears to be the best substrate. D-Lysine, D-tyrosine, and D-methionine were also good substrates. In contrast, D-glutamate, D-aspartate, L-arginine, and glycine were not detectably oxidized by the enzyme. Cysteine could not be assayed due to its nonenzymatic reaction with PMS in the enzyme reaction mixture.

DADH Recognition of Iminoarginine and Iminohistidine. Comparison of the structures of DADH in complex with iminoarginine and iminohistidine reveals the molecular basis for the relatively broad substrate specificity of this enzyme. The internal cavity of the substrate-binding site has a triangular cross section with a narrow entrance at the top, as shown in Figure 5 (DADH residues Tyr53, Gly332, and Gln336 were removed to view the internal site). The bottom of the cavity extends about 14.9 Å from loop L1 to loop L3 and 14.1 Å from loop L2 to loop L4. The depth of this substrate-binding pocket is about 10 Å from the Cα atom of Gly54 in loop L1 to the FAD O2 atom. The main chain of iminohistidine is located almost on the same plane and parallel to the isoalloxazine ring of FAD; however, the side chain of iminoarginine lies almost perpendicular to the isoalloxazine ring of FAD. The main-chain atoms of iminoarginine are very close to those of iminohistidine and form similar polar interactions with the DADH residues Tyr53, Arg222, Tyr249, Arg305, and Gly332. Since the binding pocket interactions with the main chain of the substrate are conserved, DADH has a broad substrate specificity for a variety of D-amino acids, as shown in Table 2 and reported previously (*14*). The different side-chain interactions with DADH are presumed to be responsible for the specificity differences. The longer D-arginine side chain fits well in the large substrate-binding pocket of DADH, while the smaller D-histidine cannot fill the cavity, which is consistent with the differences in catalytic activity for the two substrates.

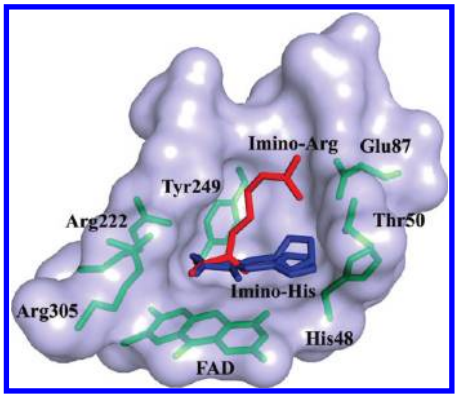

FIGURE 5: Comparison of DADH structures in complex with iminoarginine and iminohistidine. DADH active site residues (green sticks) line the interior of the substrate-binding pocket (Thr53, Gly332, and Gln336 were omitted for clarity). Iminoarginine (red) and iminohistidine (blue) bind to the active site in very distinct conformations. FAD is represented by its isoalloxazine ring in green.

Structural Comparison with Related Proteins. Determination of the crystal structure of DADH allows a detailed comparison with other mechanistically related flavin-dependent oxidoreductases. Analysis of the sequences and structures showed that DADH shares low sequence identity (< 20%) but similar three-dimensional structures with the L-proline dehydrogenase β-subunit (18.5% sequence identity, rmsd 2.2 Å for 342 Cα atoms (*26*)), heterotetrameric sarcosine oxidase (18.4% sequence identity, rmsd 2.2 Å for 339 Cα atoms (*33*)), pDAAO (17.2% sequence identity, rmsd 2.4 Å for 270 Cα atoms (*27*)), and LAAO (16.4% sequence identity, rmsd 3.0 Å for 245 Cα atoms (*29*)). For a detailed comparison of the overall structure and active site geometry, we have chosen the structures of the enzyme complexes with dicarboxylate ligands: pDAAO from pig kidney in complex with iminotryptophan (PDB entry 1DDO (*23*)) and LAAO from *Rhodococcus opacus* in complex with L-alanine (PDB entry 2JB1 (*29*)).

pDAAO and LAAO both are homodimeric enzymes formed by two subunits interacting through their helical domain or substrate-binding domain, respectively (*27*−*29*). Structural superimposition indicates that the overall structure of DADH resembles the monomer structures of pDAAO and LAAO (Figure 6). DADH and LAAO share the same topology for the FAD-binding domain in which a central β-sheet is surrounded by α-helixes on one side and a three-stranded antiparallel β-sheet on the other side. However, in the FAD-binding domain of pDAAO, an α-helix is observed instead of the three-stranded antiparallel β-sheet located in DADH (Figure 6A). All three enzymes contain a large β-pleated sheet in the substrate-binding domain, while the orientation of this β-sheet in LAAO is significantly different from those in DADH and pDAAO. Two extra β-strands are observed for LAAO at the Gly57−Cys70

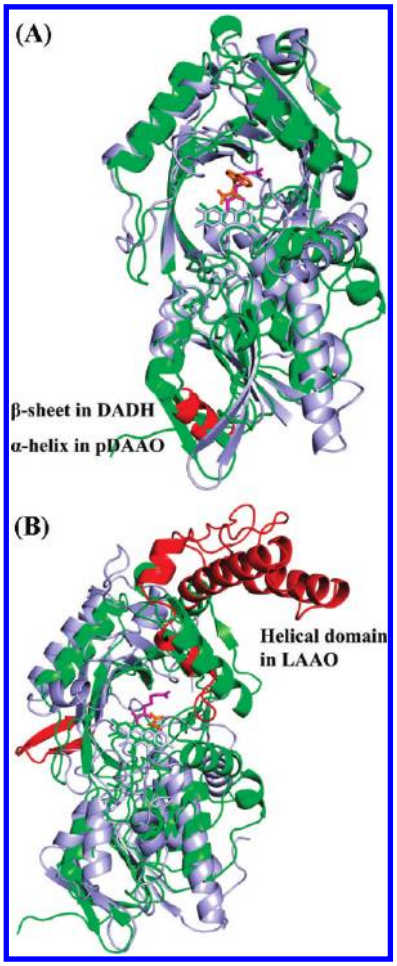

FIGURE 6: Structural comparison of DADH with pDAAO (A) and LAAO (B). DADH is shown in green cartoon representation while pDAAO and LAAO are colored in light blue with red regions indicating their major structural differences compared to DADH. FAD is represented by sticks in green and light blue corresponding to the compared structures. The ligands are iminoarginine in DADH (magenta), iminotryptophan in pDAAO (orange), and L-alanine in LAAO (orange).

region (Figure 6B). Furthermore, the helical domain involved in dimerization of LAAO is absent from the structures of DADH and pDAAO.

The substrate-binding sites of these three enzymes are all located near the *re* face of the FAD isoalloxazine ring at the interface of the FAD-binding and substrate-binding domains. Despite the opposite orientation of L-alanine bound to LAAO compared to the binding mode of ligands in the DADH and pDAAO complexes, similar protein−ligand interactions are retained among the three enzymes. The specific arrangement of active site residues is suggested to be responsible for the strict enantioselectivity of each enzyme (*23*, *27*−*29*). In the pDAAO/iminotryptophan complex, the carboxylate group of the ligand forms a salt bridge with the guanidinium side chain of Arg283 (Figure 7A). Similar interactions are formed between L-alanine and Arg84 in the structure of LAAO/L-alanine (Figure 7B). However, in the $DADH_{red}$/iminoarginine complex, this ionic interaction is replaced by interactions between the ligand and two arginines: Arg222 and Arg305. The carboxylate oxygen atoms of the ligands also form polar interactions with Tyr53, Tyr249, and Gly332 of DADH and Tyr224, Tyr228, and Gly313 of pDAAO, respectively. L-Alanine forms similar interactions with the polar residues Gln228 and Tyr371 of LAAO. The side chains of these

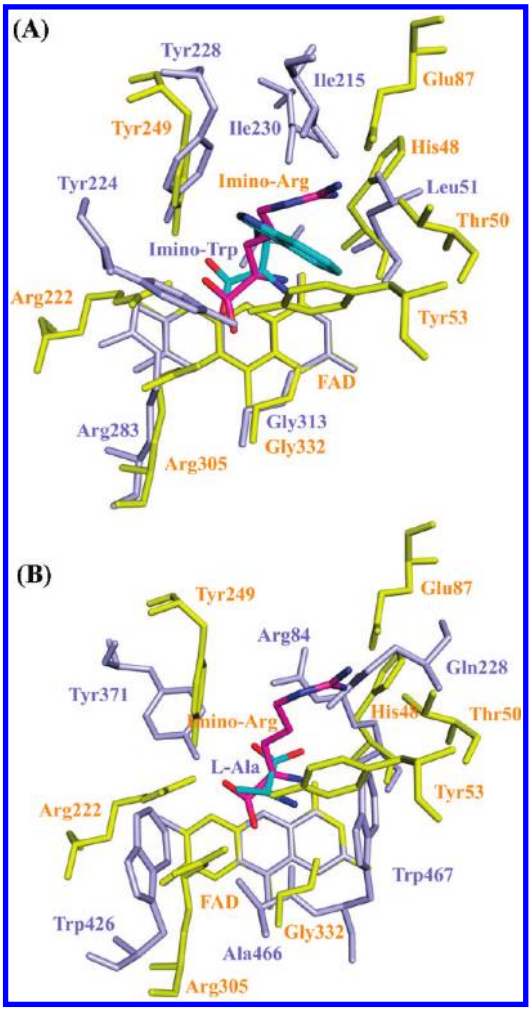

FIGURE 7: Comparison of the active sites of DADH, pDAAO, and LAAO. The active site of DADH (yellow) is superimposed on that of pDAAO (A, light blue) and LAAO (B, light blue) along the FAD isoalloxazine ring. Iminoarginine in DADH (magenta carbon atoms) and iminotryptophan in pDAAO (cyan carbon atoms) and L-alanine in LAAO (cyan) are shown as sticks. FAD is represented by its isoalloxazine ring.

ligands form distinct interactions with enzyme residues. In DADH iminoarginine forms strong ionic interactions with Glu87 and a hydrogen bond with Thr50. In contrast, in pDAAO the indole side chain of iminotryptophan is surrounded by several hydrophobic residues (Ala49, Leu51, Ile215, Ile230, and Tyr228). The short side chain of L-alanine interacts with several hydrophobic residues, Trp426, Ala466, and Trp467 of LAAO. These similarities and differences in interactions are presumed to be important determinants of their different substrate specificities.

DISCUSSION

An "Active Site Lid" Controls Substrate Accessibility. Interestingly, the atomic resolution DADH crystal structure demonstrates two conformations corresponding to the ligand-free and product-bound forms. A loop covering the active site shows a substantial conformational change between the two forms. A similar loop region described as an "active site lid" was reported in the structure of pDAAO (residues 216−228 (*27*)). It is hypothesized that this lid switches between closed and open conformations to allow substrate binding and product release (*27*). A similar "loop-and-lid" structure has been assigned in some of the glucose−methanol−choline (GMC) family members, including

glucose oxidase (residues 76−97 (*34*)), cholesterol oxidase (residues 95−109 (*35*)), pyranose 2-oxidase (residues 452−456 (*36*)), and the flavoprotein domain of cellobiose dehydrogenase (residues 289−299 (*37*)). Besides its role as a gate in opening and closing the enzyme active site, the active site lid may be important in determining the substrate specificity of DADH. The conformational change of the lid, especially for Tyr53, may allow DADH to accommodate bulky residues like D-phenylalanine or D-tryptophan. Similar interactions have been observed in pDAAO (Tyr224 (*23*)) and flavocytochrome b_2 (Tyr254 (*38*)). Furthermore, closing of the lid shields the active site and the FAD from solvent. An increase of the overall active site hydrophobicity caused by loop closure may facilitate the hydride transfer step leading to substrate oxidation in pDAAO (*23*). Similar phenomena have been described in several NAD(P)H-dependent dehydrogenases (*39*). Further insight into the function of this active site lid may be obtained by protein engineering studies on DADH.

Substrate Specificity. DADH is characterized by a broad substrate specificity, being able to oxidize basic and hydrophobic D-amino acids of various sizes (*14*). In the crystal structures iminoarginine forms a strong ionic interaction with the side chain of Glu87 and a hydrogen bond with Thr50, whereas the side chain of iminohistidine extends in a different direction and forms hydrogen bonds with His48, Thr50, and Gln336. Indeed, the steady-state kinetic data show a large k_{cat}/K_{Arg} value of 10^6 M^{-1} s^{-1} that is 1000-fold higher than the k_{cat}/K_{His} value (Table 2). Kinetic data for other D-amino acids indicate that the negatively charged side chain of Glu87 is the major determinant for the specificity of DADH for positively charged substrates D-arginine and D-lysine. Another example is seen in trypsin: residue Asp189 is responsible for its narrow selection for positively charged arginine and lysine (*40*, *41*). In addition, the hydrophobic walls (Tyr53, Met240, Val242, and Tyr249) of the DADH active site pocket create a favorable environment for the long aliphatic and unbranched parts of the basic D-arginine and D-lysine. Furthermore, D-tyrosine, D-methionine, and D-phenylalanine, which are good substrates of DADH, may form favorable van der Waals contacts with the hydrophobic walls of the active site. In contrast, DADH shows low or undetectable activities toward several D-amino acids, especially the negatively charged D-glutamate and D-aspartate.

The Ser/Ala Switch in the FAD-Binding Site. The Ser45−Ala47 region also has two conformations corresponding to the ligand-free and product-bound conformations in the DADH structure, while this region has a well-defined single conformation in the structures of $DADH_{red}$/iminoarginine and $DADH_{red}$/iminohistidine. A hydrogen bond (O_{Ser45}−$N5_{FAD}$) in the ligand-free conformation is replaced by another polar interaction (N_{Ala46}−$N5_{FAD}$) in the product-bound conformation (Figure 4C). Furthermore, interactions of the FAD N5 atom with a residue structurally equivalent to Ala46 of DADH are conserved among different FAD-dependent enzymes, such as pDAAO (Ala49 (*27*)), yeast D-amino acids oxidase (Gly52 (*42*)), L-proline dehydrogenase (Gly48 (*26*)), flavocytochrome b_2 (Ala198 (*38*)), and L-galactono-γ-lactone dehydrogenase (Ala113 (*43*)). Human DAAO shares the same sequence ($V_{47}AAGL_{51}$) with pDAAO near the *si* face of the FAD ring. However, hDAAO shows a conformational shift in this region, which has been suggested to be responsible for its low binding affinity for FAD as well as the slower rate of flavin reduction (*32*). Furthermore, substitution of the structurally equivalent Ala113 with Gly in L-galactono-γ-lactone dehydrogenase increased the reactivity of the reduced flavin with oxygen by about 400-fold (*43*). Therefore, the Ser/Ala switch in DADH might be involved in structural stability and also the enzymatic properties of this protein. Further studies are required to elucidate its function.

Structural Comparison with Related Proteins. Structural comparison of DADH with pDAAO and LAAO revealed that the active site residues of DADH are more similar to those of pDAAO (Figure 7) in agreement with their specificity for D-amino acids rather than L-amino acids (*14*). The spatial arrangement of active residues is critically related to the enzyme enantiomeric selectivity. A mirror-symmetrical relationship of active sites has been described among enzymes with opposite stereospecificities, and two different modes have been reported. One is observed between pDAAO and flavocytochrome b_2, in which the active sites of the two enzymes are mirrored through the plane of isoalloxazine (on the *re* side in pDAAO, on the *si* side in flavocytochrome b_2) (*27*). Another situation is that the substrate-binding sites are mirrored through the plane perpendicular to the isoalloxazine ring, which is observed in the comparison between pDAAO and LAAO (*28*). The active site of DADH is highly similar to that of pDAAO and mirror-symmetrically related to that of LAAO (Figure 7). This observation is in agreement with the kinetic study described previously (*14*) and in this paper showing that DADH can oxidize a variety of D-amino acids but not L-arginine. A similar active site arrangement has been observed in other flavoenzymes like glycolate oxidase (*44*), L-glutamate oxidase (*45*) and L-aspartate oxidase (*46*), suggesting these enzymes employ a common mechanism to control enantioselectivity.

In addition to their specificity toward different enantiomers of amino acids, DADH, pDAAO, and LAAO display other distinct features. For example, the ligands are held in the active site by a salt bridge formed with an arginine in pDAAO and LAAO, while two active site arginines are involved in DADH. The active sites of DADH and pDAAO are covered by a loop termed the "active site lid". This feature was not reported in the structure of LAAO, and a funnel-shaped entrance for substrate binding was proposed instead (*47*). In addition to the polar interactions between the ligands and the enzyme active site residues, a hydrophobic environment has been observed in all three enzymes. In fact, all of the enzymes interact with a wide range of hydrophobic amino acids (*14*, *23*, *48*). Overall, the different composition and arrangement of active site residues determine differences in substrate specificity, while critical interactions for catalysis are conserved among these mechanistically related enzymes.

Conclusions. Comparison of the crystal structures of DADH and its complexes with iminoarginine and iminohistidine has highlighted important structural differences that rationalize the catalytic activities and substrate specificity of the enzyme. The imino products of D-arginine and D-histidine bind to the active site in very distinct side-chain conformations. Glu87 forms strong electrostatic interactions with iminoarginine, which is likely responsible for the high selectivity of DADH for positively charged residues like D-arginine and D-lysine. A loop region has been designated as an active site lid controlling the substrate accessibility to the active site, similar to those reported in other flavin-dependent enzymes. Structural comparison of DADH with other related flavin-dependent enzymes reveals that the spatial arrangement of active site residues is essential for the differences in enzyme enantioselectivity, while some specific

interactions needed for catalysis are conserved among the enzymes. Overall, the high-resolution structures for DADH described in this study will provide new guidelines for future studies of similar flavin-dependent enzymes.

ACKNOWLEDGMENT

We thank Dr. Johnson Agniswamy and Dr. Yuan-Fang Wang for providing help with refinement and valuable discussions. We are especially grateful for the assistance of Dr. Zheng-Qing Fu and the staff at the SER-CAT beamline at the Advanced Photon Source, Argonne National Laboratory, for assistance during X-ray data collection. Use of the Advanced Photon Source was supported by the U.S. Department of Energy, Office of Science, Office of Basic Energy Sciences, under Contract No. W-31-109-Eng-38.

REFERENCES

1. Pollegioni, L., Piubelli, L., Sacchi, S., Pilone, M. S., and Molla, G. (2007) Physiological functions of D-amino acid oxidases: from yeast to humans. *Cell. Mol. Life Sci. 64*, 1373–1394.
2. Kolodkin-Gal, I., Romero, D., Cao, S., Clardy, J., Kolter, R., and Losick, R. (2010) D-Amino acids trigger biofilm disassembly. *Science 328*, 627–629.
3. Yoshimura, T., and Esak, N. (2003) Amino acid racemases: functions and mechanisms. *J. Biosci. Bioeng. 96*, 103–109.
4. Dunlop, D. S., Neidle, A., McHale, D., Dunlop, D. M., and Lajtha, A. (1986) The presence of free D-aspartic acid in rodents and man. *Biochem. Biophys. Res. Commun. 141*, 27–32.
5. Hashimoto, A., Nishikawa, T., Oka, T., and Takahashi, K. (1993) Endogenous D-serine in rat brain: N-methyl-D-aspartate receptor-related distribution and aging. *J. Neurochem. 60*, 783–786.
6. Snyder, S. H., and Kim, P. M. (2000) D-amino acids as putative neurotransmitters: focus on D-serine. *Neurochem. Res. 25*, 553–560.
7. Wolosker, H. (2007) NMDA receptor regulation by D-serine: new findings and perspectives. *Mol. Neurobiol. 36*, 152–164.
8. Olsiewski, P. J., Kaczorowski, G. J., and Walsh, C. (1980) Purification and properties of D-amino acid dehydrogenase, an inducible membrane-bound iron-sulfur flavoenzyme from *Escherichia coli* B. *J. Biol. Chem. 255*, 4487–4494.
9. Raunio, R. P., and Jenkins, W. T. (1973) D-alanine oxidase form *Escherichia coli*: localization and induction by L-alanine. *J. Bacteriol. 115*, 560–566.
10. David, H. L., Clavel-Seres, S., Clement, F., Lazlo, A., and Rastogi, N. (1989) Methionine as methyl-group donor in the synthesis of *Mycobacterium avium* envelope lipids, and its inhibition by DL-ethionine, D-norleucine and DL-norleucine. *Acta Leprol. 7* (Suppl. 1), 77–80.
11. Haas, D., Matsumoto, H., Moretti, P., Stalon, V., and Mercenier, A. (1984) Arginine degradation in *Pseudomonas aeruginosa* mutants blocked in two arginine catabolic pathways. *Mol. Gen. Genet. 193*, 437–444.
12. Lu, C. D. (2006) Pathways and regulation of bacterial arginine metabolism and perspectives for obtaining arginine overproducing strains. *Appl. Microbiol. Biotechnol. 70*, 261–272.
13. Li, C., and Lu, C. D. (2009) Arginine racemization by coupled catabolic and anabolic dehydrogenases. *Proc. Natl. Acad. Sci. U.S. A. 106*, 906–911.
14. Li, C., Yao, X., and Lu, C. D. (2010) Regulation of the dauBAR operon and characterization of D-amino acid dehydrogenase DauA in arginine and lysine catabolism of *Pseudomonas aeruginosa* PAO1. *Microbiology 156*, 60–71.
15. Liu, P., Wang, Y. F., Ewis, H. E., Abdelal, A. T., Lu, C. D., Harrison, R. W., and Weber, I. T. (2004) Covalent reaction intermediate revealed in crystal structure of the *Geobacillus stearothermophilus* carboxylesterase Est30. *J. Mol. Biol. 342*, 551–561.
16. Otwinowski, Z., and Minor, W. (1997) Processing of X-ray diffraction data collected in oscillation mode. *Methods Enzymol. 267*, 307–326.
17. Fu, Z. Q., Rose, J., and Wang, B. C. (2005) SGXPro: a parallel workflow engine enabling optimization of program performance and automation of structure determination. *Acta Crystallogr., Sect. D: Biol. Crystallogr. 61*, 951–959.
18. Lamzin, V. S., and Wilson, K. S. (1993) Automated refinement of protein models. *Acta Crystallogr., Sect. D: Biol. Crystallogr. 49*, 129–147.
19. McCoy, A. J., Grosse-Kunstleve, R. W., Storoni, L. C., and Read, R. J. (2005) Likelihood-enhanced fast translation functions. *Acta Crystallogr., Sect. D: Biol. Crystallogr. 61*, 458–464.
20. Potterton, E., Briggs, P., Turkenburg, M., and Dodson, E. (2003) A graphical user interface to the CCP4 program suite. *Acta Crystallogr., Sect. D: Biol. Crystallogr. 59*, 1131–1137.
21. Sheldrick, G. M., and Schneider, T. R. (1997) SHELXL: high-resolution refinement. *Methods Enzymol. 277*, 319–343.
22. Emsley, P., and Cowtan, K. (2004) Coot: model-building tools for molecular graphics. *Acta Crystallogr., Sect. D: Biol. Crystallogr. 60*, 2126–2132.
23. Todone, F., Vanoni, M. A., Mozzarelli, A., Bolognesi, M., Coda, A., Curti, B., and Mattevi, A. (1997) Active site plasticity in D-amino acid oxidase: a crystallographic analysis. *Biochemistry 36*, 5853–5860.
24. Altschul, S. F., Madden, T. L., Schaffer, A. A., Zhang, J., Zhang, Z., Miller, W., and Lipman, D. J. (1997) Gapped BLAST and PSI-BLAST: a new generation of protein database search programs. *Nucleic Acids Res. 25*, 3389–3402.
25. Krissinel, E., and Henrick, K. (2004) Secondary-structure matching (SSM), a new tool for fast protein structure alignment in three dimensions. *Acta Crystallogr., Sect. D: Biol. Crystallogr. 60*, 2256–2268.
26. Tsuge, H., Kawakami, R., Sakuraba, H., Ago, H., Miyano, M., Aki, K., Katunuma, N., and Ohshima, T. (2005) Crystal structure of a novel FAD-, FMN-, and ATP-containing L-proline dehydrogenase complex from *Pyrococcus horikoshii*. *J. Biol. Chem. 280*, 31045–31049.
27. Mattevi, A., Vanoni, M. A., Todone, F., Rizzi, M., Teplyakov, A., Coda, A., Bolognesi, M., and Curti, B. (1996) Crystal structure of D-amino acid oxidase: a case of active site mirror-image convergent evolution with flavocytochrome b_2. *Proc. Natl. Acad. Sci. U.S.A. 93*, 7496–7501.
28. Pawelek, P. D., Cheah, J., Coulombe, R., Macheroux, P., Ghisla, S., and Vrielink, A. (2000) The structure of L-amino acid oxidase reveals the substrate trajectory into an enantiomerically conserved active site. *EMBO J. 19*, 4204–4215.
29. Faust, A., Niefind, K., Hummel, W., and Schomburg, D. (2007) The structure of a bacterial L-amino acid oxidase from *Rhodococcus opacus* gives new evidence for the hydride mechanism for dehydrogenation. *J. Mol. Biol. 367*, 234–248.
30. Dym, O., and Eisenberg, D. (2001) Sequence-structure analysis of FAD-containing proteins. *Protein Sci. 10*, 1712–1728.
31. Dixon, D. A., Lindner, D. L., Branchaud, B., and Lipscomb, W. N. (1979) Conformations and electronic structures of oxidized and reduced isoalloxazine. *Biochemistry 18*, 5770–5775.
32. Kawazoe, T., Tsuge, H., Pilone, M. S., and Fukui, K. (2006) Crystal structure of human D-amino acid oxidase: context-dependent variability of the backbone conformation of the VAAGL hydrophobic stretch located at the si-face of the flavin ring. *Protein Sci. 15*, 2708–2717.
33. Chen, Z. W., Hassan-Abdulah, A., Zhao, G., Jorns, M. S., and Mathews, F. S. (2006) Heterotetrameric sarcosine oxidase: structure of a diflavin metalloenzyme at 1.85 Å resolution. *J. Mol. Biol. 360*, 1000–1018.
34. Wohlfahrt, G., Witt, S., Hendle, J., Schomburg, D., Kalisz, H. M., and Hecht, H. J. (1999) 1.8 and 1.9 Å resolution structures of the *Penicillium amagasakiense* and *Aspergillus niger* glucose oxidases as a basis for modelling substrate complexes. *Acta Crystallogr., Sect. D: Biol. Crystallogr. 55*, 969–977.
35. Li, J., Vrielink, A., Brick, P., and Blow, D. M. (1993) Crystal structure of cholesterol oxidase complexed with a steroid substrate: implications for flavin adenine dinucleotide dependent alcohol oxidases. *Biochemistry 32*, 11507–11515.
36. Hallberg, B. M., Leitner, C., Haltrich, D., and Divne, C. (2004) Crystal structure of the 270 kDa homotetrameric lignin-degrading enzyme pyranose 2-oxidase. *J. Mol. Biol. 341*, 781–796.
37. Hallberg, B. M., Henriksson, G., Pettersson, G., and Divne, C. (2002) Crystal structure of the flavoprotein domain of the extracellular flavocytochrome cellobiose dehydrogenase. *J. Mol. Biol. 315*, 421–434.
38. Xia, Z. X., and Mathews, F. S. (1990) Molecular structure of flavocytochrome b_2 at 2.4 Å resolution. *J. Mol. Biol. 212*, 837–863.
39. Stoll, V. S., Kimber, M. S., and Pai, E. F. (1996) Insights into substrate binding by D-2-ketoacid dehydrogenases from the structure of *Lactobacillus pentosus* D-lactate dehydrogenase. *Structure 4*, 437–447.
40. Lu, W., Apostol, I., Qasim, M. A., Warne, N., Wynn, R., Zhang, W. L., Anderson, S., Chiang, Y. W., Ogin, E., Rothberg, I., Ryan, K., and Laskowski, M. (1997) Binding of amino acid side-chains to S1 cavities of serine proteinases. *J. Mol. Biol. 266*, 441–461.

41. Brandsdal, B. O., Aqvist, J., and Smalas, A. O. (2001) Computational analysis of binding of P1 variants to trypsin. *Protein Sci. 10*, 1584–1595.
42. Umhau, S., Pollegioni, L., Molla, G., Diederichs, K., Welte, W., Pilone, M. S., and Ghisla, S. (2000) The x-ray structure of D-amino acid oxidase at very high resolution identifies the chemical mechanism of flavin-dependent substrate dehydrogenation. *Proc. Natl. Acad. Sci. U.S.A. 97*, 12463–12468.
43. Leferink, N. G., Fraaije, M. W., Joosten, H. J., Schaap, P. J., Mattevi, A., and van Berkel, W. J. (2009) Identification of a gatekeeper residue that prevents dehydrogenases from acting as oxidases. *J. Biol. Chem. 284*, 4392–4397.
44. Lindqvist, Y. (1989) Refined structure of spinach glycolate oxidase at 2 Å resolution. *J. Mol. Biol. 209*, 151–166.
45. Arima, J., Sasaki, C., Sakaguchi, C., Mizuno, H., Tamura, T., Kashima, A., Kusakabe, H., Sugio, S., and Inagaki, K. (2009) Structural characterization of L-glutamate oxidase from *Streptomyces* sp. X-119-6. *FEBS J. 276*, 3894–3903.
46. Bossi, R. T., Negri, A., Tedeschi, G., and Mattevi, A. (2002) Structure of FAD-bound L-aspartate oxidase: insight into substrate specificity and catalysis. *Biochemistry 41*, 3018–3024.
47. Moustafa, I. M., Foster, S., Lyubimov, A. Y., and Vrielink, A. (2006) Crystal structure of LAAO from *Calloselasma rhodostoma* with an L-phenylalanine substrate: insights into structure and mechanism. *J. Mol. Biol. 364*, 991–1002.
48. Massey, V., and Curti, B. (1967) On the reaction mechanism of *Crotalus adamanteus* L-amino acid oxidase. *J. Biol. Chem. 242*, 1259–1264.